



**HAL**  
open science

# Modeling of Photovoltaic System with Modified Incremental Conductance Algorithm for Fast Changes of Irradiance

Saad Motahhir, Abdelaziz El Ghzizal, Souad Sebti, Aziz Derouich

► **To cite this version:**

Saad Motahhir, Abdelaziz El Ghzizal, Souad Sebti, Aziz Derouich. Modeling of Photovoltaic System with Modified Incremental Conductance Algorithm for Fast Changes of Irradiance. International Journal of Photoenergy, 2018, 2018, pp.1 - 13. 10.1155/2018/3286479 . hal-01767022

**HAL Id: hal-01767022**

**<https://hal.science/hal-01767022>**

Submitted on 15 Apr 2018

**HAL** is a multi-disciplinary open access archive for the deposit and dissemination of scientific research documents, whether they are published or not. The documents may come from teaching and research institutions in France or abroad, or from public or private research centers.

L'archive ouverte pluridisciplinaire **HAL**, est destinée au dépôt et à la diffusion de documents scientifiques de niveau recherche, publiés ou non, émanant des établissements d'enseignement et de recherche français ou étrangers, des laboratoires publics ou privés.

## Research Article

# Modeling of Photovoltaic System with Modified Incremental Conductance Algorithm for Fast Changes of Irradiance

Saad Motahhir , Abdelaziz El Ghzizal, Souad Sebti, and Aziz Derouich

Laboratory of Production Engineering, Energy and Sustainable Development, Higher School of Technology, SMBA University, Fez, Morocco

Correspondence should be addressed to Saad Motahhir; [saad.motahhir@usmba.ac.ma](mailto:saad.motahhir@usmba.ac.ma)

Received 6 September 2017; Accepted 7 December 2017; Published 13 March 2018

Academic Editor: Philippe Poggi

Copyright © 2018 Saad Motahhir et al. This is an open access article distributed under the Creative Commons Attribution License, which permits unrestricted use, distribution, and reproduction in any medium, provided the original work is properly cited.

The first objective of this work is to determine some of the performance parameters characterizing the behavior of a particular photovoltaic (PV) panels that are not normally provided in the manufacturers' specifications. These provide the basis for developing a simple model for the electrical behavior of the PV panel. Next, using this model, the effects of varying solar irradiation, temperature, series and shunt resistances, and partial shading on the output of the PV panel are presented. In addition, the PV panel model is used to configure a large photovoltaic array. Next, a boost converter for the PV panel is designed. This converter is put between the panel and the load in order to control it by means of a maximum power point tracking (MPPT) controller. The MPPT used is based on incremental conductance (INC), and it is demonstrated here that this technique does not respond accurately when solar irradiation is increased. To investigate this, a modified incremental conductance technique is presented in this paper. It is shown that this system does respond accurately and reduces the steady-state oscillations when solar irradiation is increased. Finally, simulations of the conventional and modified algorithm are compared, and the results show that the modified algorithm provides an accurate response to a sudden increase in solar irradiation.

## 1. Introduction

The energy generated by the PV systems depends on various parameters, either environmental as temperature and irradiance or internal parameters of the PV panel, namely, the series and shunt resistors [1, 2]. Thus, the load imposes its own characteristic on the output power [3]. Therefore, in order to predict and analyze the effect of these parameters on the PV power, the model of the PV panel should be previously studied and achieved, and this model should be in accordance with the real comportment of the PV panel. Therefore, different models were proposed in the literature. In [4], a single diode model is used; in [5], a two-diode model is proposed to illustrate the influence of the recombination of carriers; and in [6], a model of three diodes is used to present the effects which are neglected by the two-diode model. However, the single-diode model is the most adopted due to its good simplicity and accuracy [7]. Moreover, manufacturers of PV panels offer only some characteristics. But other characteristics required to model PV panel are missed in the

datasheet, as the photocurrent, the diode saturation current, the series and shunt resistors, and the ideality factor [8]. Hence, in [7, 9, 10], researchers have proposed different methods to extract the lacking characteristics based on the datasheet values, but these methods require an implementation and this can increase the time spent in the development of a PV application. Therefore, this paper aims firstly to extract lacking parameters in the manufacturers' datasheet by using a simple tool provided by MathWorks [11] and then model the PV panel. The single-diode model is used in this work because it gives a high compromise between accuracy and simplicity [12], and several researchers have used it in their works [13, 14]. In addition, this work shows the effect of parameters that may change the performance of the PV panel. Then, this model will be a platform to design a PV array.

On the other side, the maximization of the PV power always remains a major challenge. Researchers have proposed different MPPT algorithms to maximize PV power, namely, FSCC, FOCV, fuzzy logic, neural network, P&O,

and INC [15, 16]. FSCC and FOCV are the simplest MPPT algorithms, which are based on the linearity of short-circuit current or open-circuit voltage to the maximum power point current or voltage. However, these techniques isolate the PV panel to measure the short-circuit current or open-circuit voltage. Therefore, the loss of energy is increased due to the periodic isolation of the panel [17]. Alternatively, fuzzy logic and neural network obtain a consistent MPPT technique due to their ability to treat the nonlinearity of the PV panel. But the main drawback of fuzzy logic is that the effectiveness of this algorithm depends a lot on choosing the right error computation and an appropriate rule base [18]. In addition, neural network presents many disadvantages like the fact that the data needed for the training process have to be specifically acquired for every PV array and location, and also, the PV characteristics change with time, so the neural network has to be periodically trained [18]. On the other hand, P&O and INC are mostly used. These techniques use the ( $P$ - $V$ ) characteristic of the PV panel. For P&O, steady-state oscillations occur after the MPP is found due to the perturbation made by this technique to maintain the MPP, which in turn increases the loss of power [19]. For INC, it is founded in the fact that slope of  $P$ - $V$  characteristic is zero at the maximum power, and theoretically, there is no perturbation after the MPP is found. Therefore, oscillations are minimized. However, during implementation, the zero value is hardly found on the slope of the  $P$ - $V$  characteristic due to the truncation error in digital processing. Thus, the INC technique can make an inaccurate response when the irradiation is suddenly increased [20]. Therefore, this work aims also to propose and implement a modified INC algorithm, which can overcome the wrong response made by the conventional INC algorithm when the irradiance is suddenly increased. Therefore, this work proposes a new technique to detect the increase in solar irradiation. The variation of voltage ( $\Delta V$ ) and current ( $\Delta I$ ) are used to identify the increase in irradiation instead of the slope ( $\Delta P/\Delta V$ ) of the  $P$ - $V$  characteristic. The modified algorithm detects the increase of irradiance and makes a correct decision. Moreover, a mini error is accepted to admit that the slope is near to zero and minimize the steady-state oscillations.

This paper is structured as follows. Following the introduction, Section 2 presents the modeling of PV panel and array and presents the impact of different environmental and internal parameters. Section 3 presents the design of the boost converter, the conventional algorithm, and the proposed algorithm.

## 2. Modeling of PV Panel and Array

**2.1. Model of PV Panel.** As shown in Figure 1, the single-diode model of PV panel can be presented by a photocurrent source and a diode connected with series and shunt resistances. The mathematical model of the PV panel can be presented by the following equations [19]:

$$I = I_{ph} - I_s \left( \exp \frac{q(V + R_s I)}{aKT N_s} - 1 \right) - \frac{(V + IR_s)}{R_{sh}}, \quad (1)$$

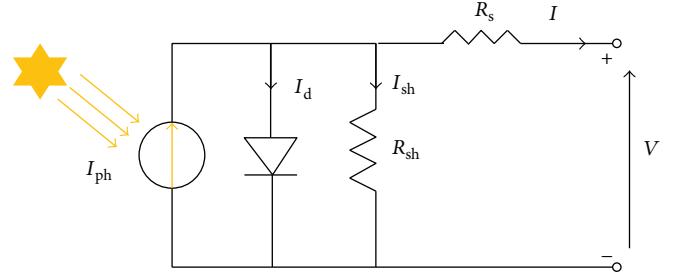


FIGURE 1: PV panel equivalent circuit.

TABLE 1: Characteristics of MSX-60 PV panel at STC.

PV panel parameters	Values
Maximum power, $P_{max}$	60 W
Maximum power voltage, $V_{mp}$	17.1 V
Maximum power current, $I_{mp}$	3.5 A
Short-circuit current, $I_{sc}$	3.8 A
Open-circuit voltage, $V_{CO}$	21.1 V
Voltage/temp. coefficient, $K_V$	-0.38%/°C
Current/temp. coefficient, $K_I$	0.065%/°C
The number of cells, $N_s$	36

$$I_{ph} = (I_{sc} + K_i(T - 298.15)) \frac{G}{1000}, \quad (2)$$

$$I_s = \frac{I_{sc} + K_i(T - 298.15)}{\exp(q((V_{OC} + K_V(T - 298.15))/aKT N_s)) - 1}. \quad (3)$$

Hence, the physical behavior of the PV panel depends on the shunt and series resistances, solar irradiation, and temperature. Therefore, in this work, the impact of these parameters on the output of the PV panel is investigated.

The panel used in this work is MSX-60 panel, and as presented in Table 1, the datasheet of PV panel provides only some characteristics of PV panel. Thus, other characteristics required to model PV panel are missed in the datasheet, as the photocurrent, the diode saturation current, the series and shunt resistors, and the ideality factor. Hence, researchers have proposed different methods to extract the lacking characteristics based on the datasheet [7, 9, 10]. But these methods require an implementation and this can increase the time spent in the development of a PV system. Therefore, this work aims firstly to extract these parameters by using a simple tool provided by MathWorks which is "PV array;" the latter is available in Simulink 2015 or later [11]. Hence, as shown in Figure 2, we only have to set the datasheet values and automatically it will generate the lacking parameters.

Equations (1), (2), and (3) are modeled using PSIM (software for power electronics simulation), and Figure 3 presents the PSIM model.

Figure 4 shows the  $I$ - $V$  and  $P$ - $V$  curves of experimental and PSIM model under STC. The experimental data  $P(V)$  and  $I(V)$  are taken from the manufactured datasheet [21].

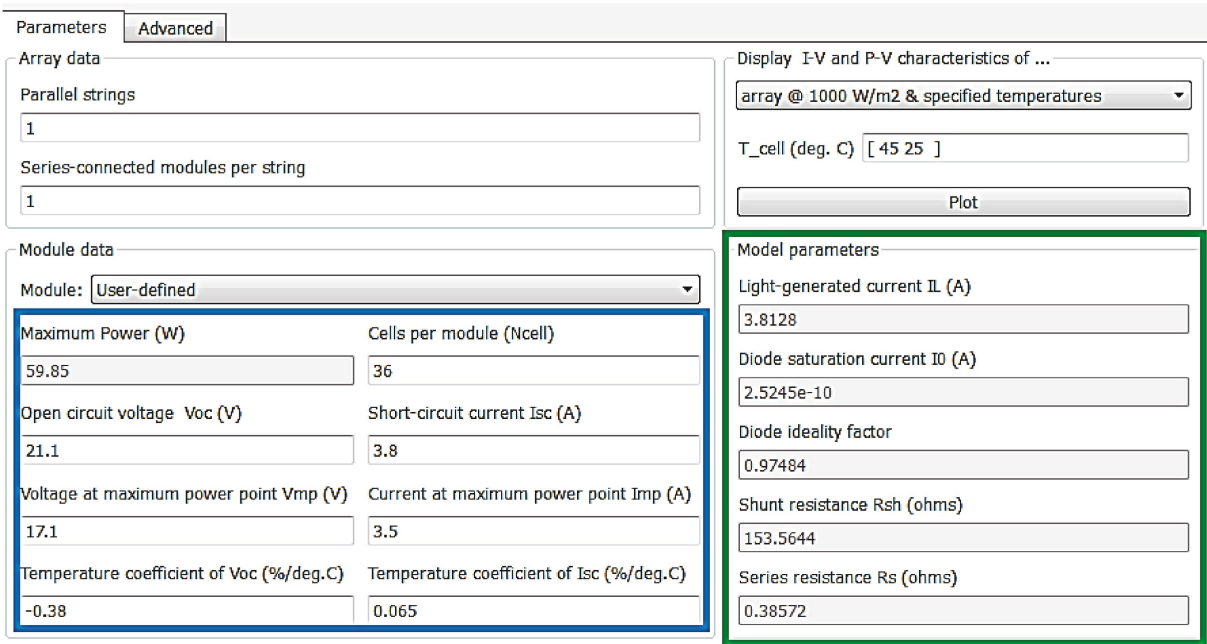


FIGURE 2: PV array tool.

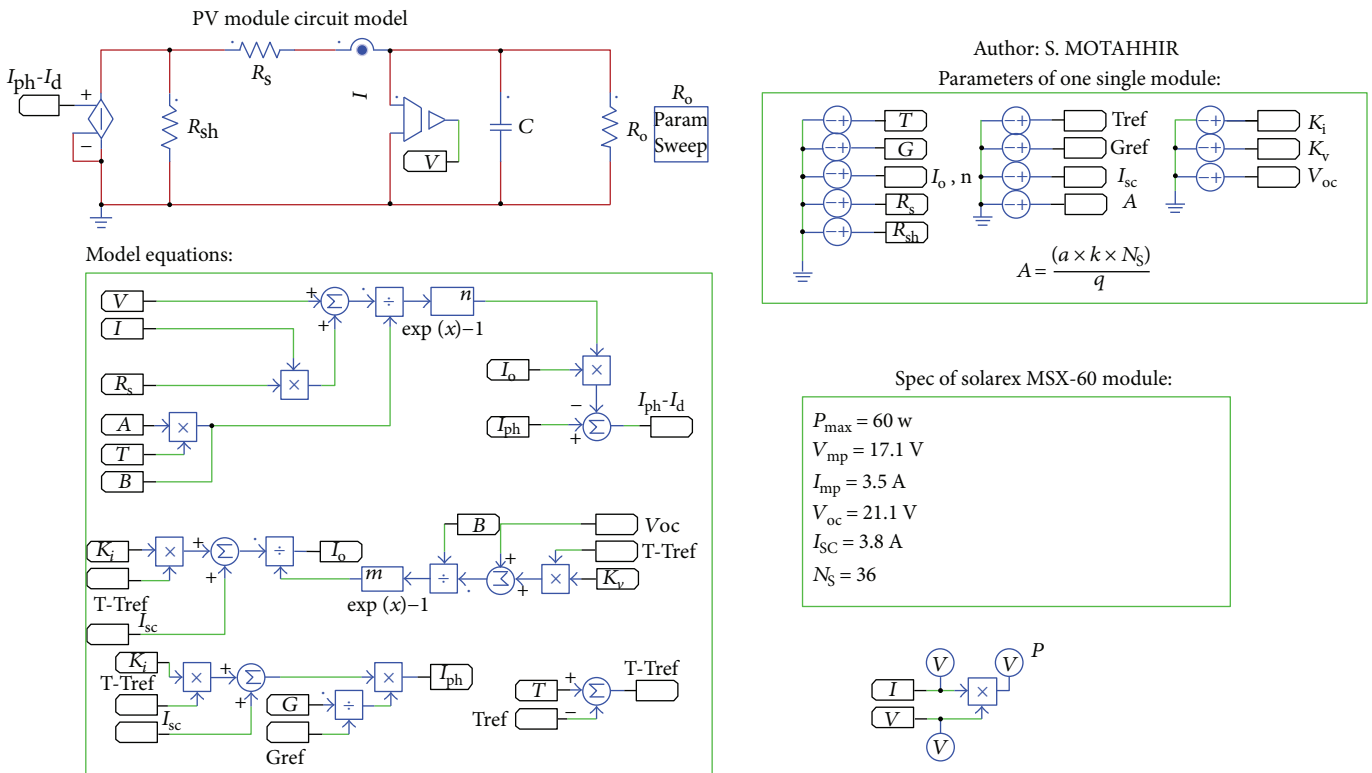


FIGURE 3: PV panel PSIM model.

And as presented, the model data are in accordance with the experimental data both in the current and power curves.

2.2. Effect of Solar Irradiation Variation. Figure 3 contains the model of the three equations: one of these equations computes the photocurrent based on temperature and

irradiance (2). The model of this equation is presented in Figure 5, and Figure 6 presents  $I-V$  and  $P-V$  curves for different values of solar irradiation.

As presented in Figure 6, the PV panel current depends heavily on solar irradiation. However, the voltage increases just by 1 V once the irradiance is increased from  $400 \text{ W/m}^2$

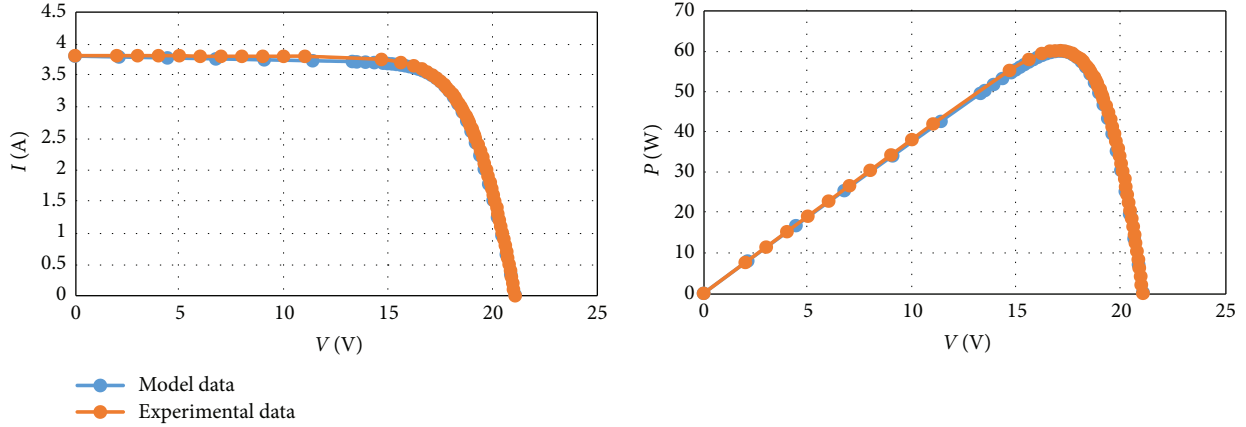


FIGURE 4:  $I$ - $V$  and  $P$ - $V$  characteristics of model and experimental data.

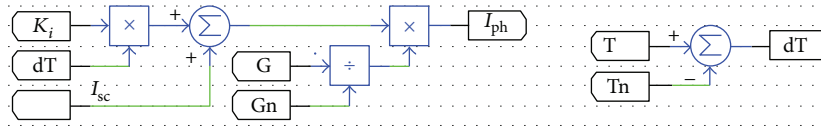


FIGURE 5: Model of (2).

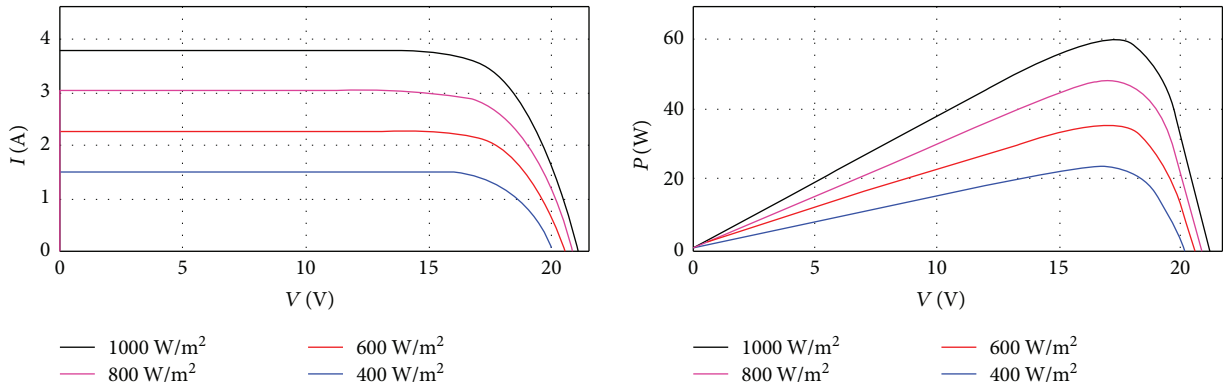


FIGURE 6:  $I$ - $V$  and  $P$ - $V$  curves for different values of irradiance.

to  $1000 \text{ W/m}^2$ . Therefore, the irradiance change affects heavily the PV panel current.

**2.3. Effect of the Temperature Variation.** Figure 3 contains also the modeling of (3), which computes the diode saturation current based on the temperature. The model of this equation is shown in Figure 7, and Figure 8 shows the  $I$ - $V$  and  $P$ - $V$  curves for different values of temperature.

Generally, as shown in Figure 8, for a fixed solar irradiation and when the temperature increases, the open-circuit voltage decreases and the short-circuit current increases with a little value. Therefore, the temperature change affects strongly the PV panel voltage.

**2.4. Effect of Series Resistor Variation.** The series resistor value is very small, and it may be neglected in some cases. Nevertheless, to make the appropriate model for any PV panel, it is recommended to make a variation of this resistor

and show its effect on the PV panel output. As shown in Figure 9, the change of the series resistor results on the deviation of the MPP.

The simulation was made for three values of series resistance ( $1 \text{ m}\Omega$ ,  $4 \text{ m}\Omega$ , and  $8 \text{ m}\Omega$ ). Moreover, as shown in Figure 9, the upper values of series resistance decrease the output power. In addition, the fill factor presented by (4) decreases as series resistance increases [22].

$$FF = \frac{P_{\max}}{V_{OC}I_{SC}}. \tag{4}$$

**2.5. Effect of Shunt Resistor Variation.** As presented in Figure 10,  $R_{sh}$  should be quite large for a good fill factor. In fact, when  $R_{sh}$  is small, the current collapses more strongly, then the loss of power is high, and the fill factor is low. Therefore,  $R_{sh}$  of any PV panel should be large enough for a good efficiency.

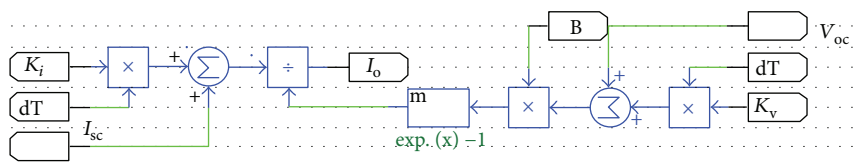


FIGURE 7: Model of (3).

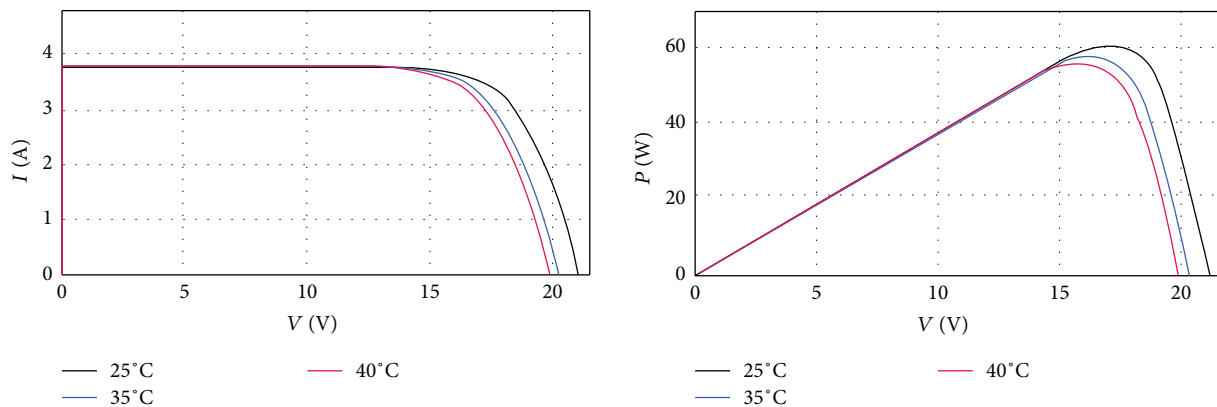


FIGURE 8:  $I$ - $V$  and  $P$ - $V$  curves for different values of temperature.

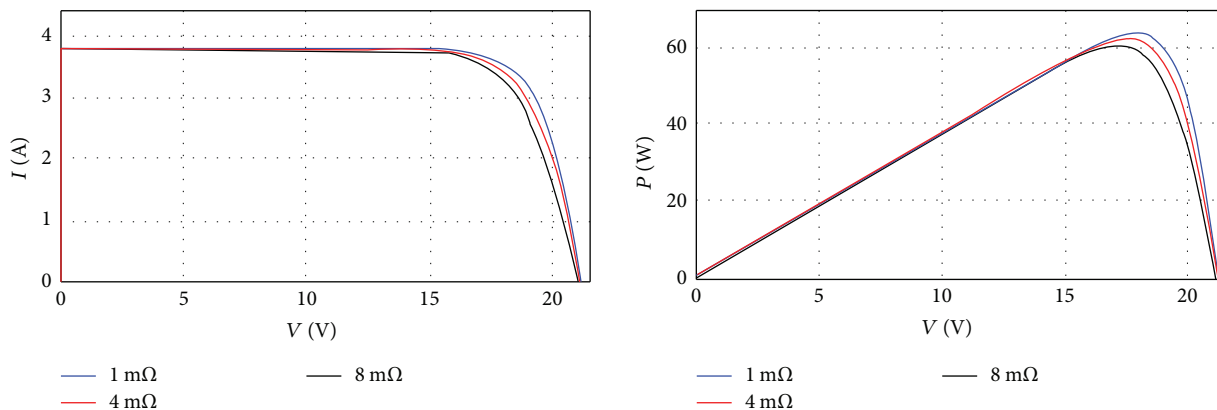


FIGURE 9:  $I$ - $V$  and  $P$ - $V$  curves for different values of  $R_s$ .

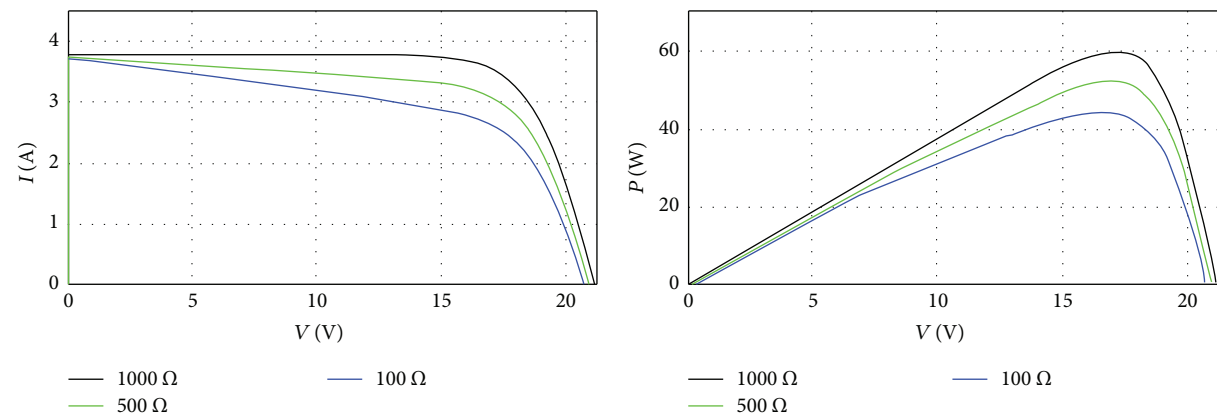


FIGURE 10:  $I$ - $V$  and  $P$ - $V$  curves for different values of  $R_{sh}$ .

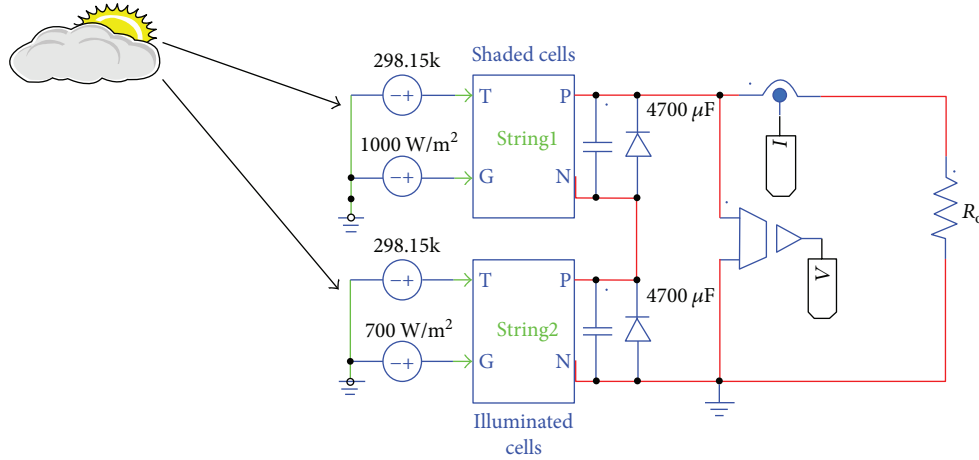
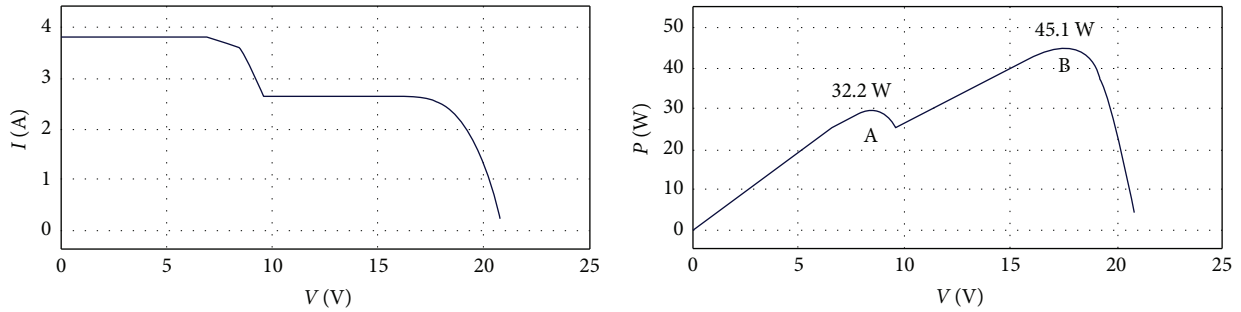


FIGURE 11: PV panel under nonuniform irradiation.

FIGURE 12:  $I$ - $V$  and  $P$ - $V$  characteristics of the PV panel under nonuniform irradiation.

**2.6. Effect of Shading.** Partial shading also presents a major impact on PV output power. When the insolation received by a part of the PV panel (shaded cells) is less than the insolation received by another part (illuminated cells), the current generated by the illuminated cells is greater than the current produced by the shaded cells; this mismatch makes the diode of shaded cells reverse biased; consequently, the power will be lost in the shaded cells and that may cause a hot spot problem which is the reason of permanent damage to the PV panel [19]. Hence, in order to overcome this problem, the bypass diodes can be connected in parallel with PV cells [19].

To simulate the effect of shading, a bypass diode is associated with each string of the panel, and it should be mentioned that the panel used includes two strings and each string is a set of 18 cells. Thus, as shown in Figure 11, the first string is exposed by  $1000 \text{ W/m}^2$  and the second string by  $700 \text{ W/m}^2$ .

Under uniform irradiation, the bypass diodes have no impact because they are reversely biased. But under shading, the current flows through the bypass diode instead of the shaded string because the bypass diode is directly biased, and as a result, no power will be lost in the shaded cells and only the illuminated cells generate power. Figure 12 shows the effect of bypass diodes on the PV panel characteristics and as presented, multiple peaks may occur on the  $P$ - $V$  curve; as in this case, there are two peaks, point A which is the global peak and point B which is the local peak.

Therefore, conventional MPPT algorithms are unable to track the global peak which is the real MPP [19].

**2.7. Photovoltaic Array.** To get benefit from the model developed, a PV array of 18 PV panels has been built in order to supply a solar pumping station, not studied in this paper. Therefore, as shown in Figure 13, three strings of six PV panels have been linked in parallel and each group is composed of six panels in series.

The model of the PV array has been achieved on PSIM, and simulation result obtained is presented in Figure 14.

As presented in Figure 14, the panels connected in parallel increase the current and the panels connected in series increase the voltage. However, as discussed in the previous section, this connection between panels can lead to hot spot problem when the insolation received by a part of the PV array (shaded panels) is less than the insolation received by another part (illuminated panels).

### 3. Modified INC Algorithm with Boost Converter

PV panel provides  $I$ - $V$  and  $P$ - $V$  curves presented in Figure 15; these curves highlight one point where the power is maximum. As presented above, this point depends on solar irradiation and temperature. Moreover, as presented in Figure 15, in general, load's characteristic is different from the MPP. Therefore, the boost converter controlled by a duty

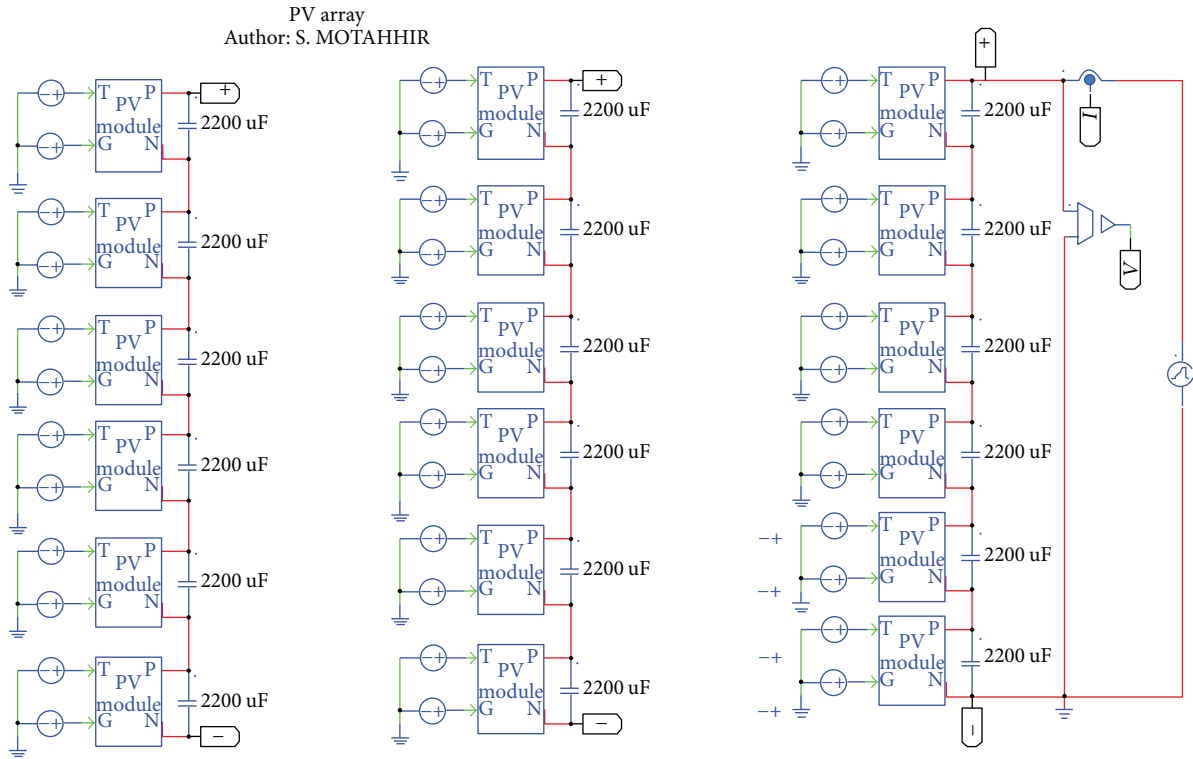


FIGURE 13: PV array model.

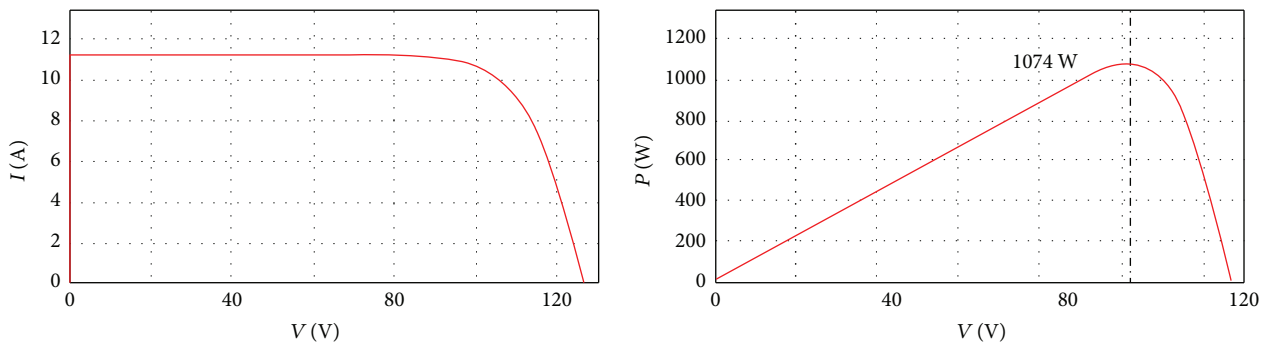


FIGURE 14:  $I$ - $V$  and  $P$ - $V$  curves of the PV array.

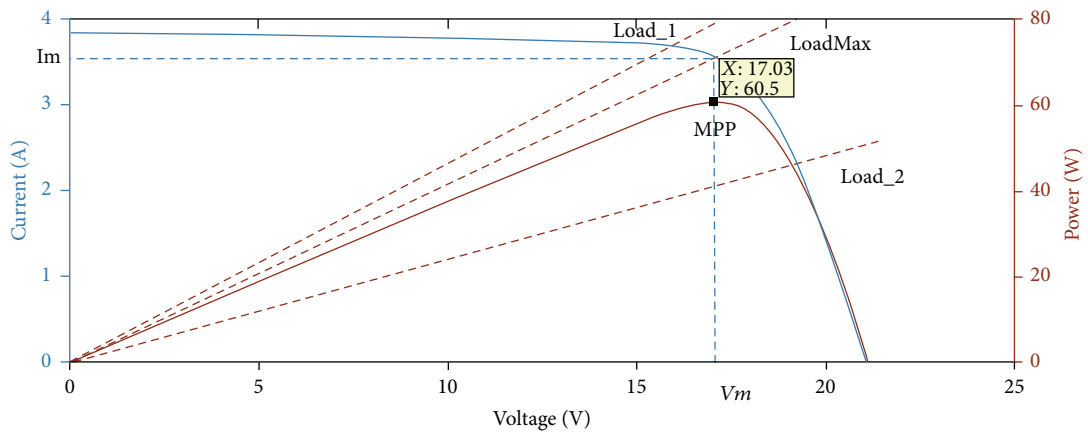


FIGURE 15: The impact of load on  $I$ - $V$  and  $P$ - $V$  characteristics.

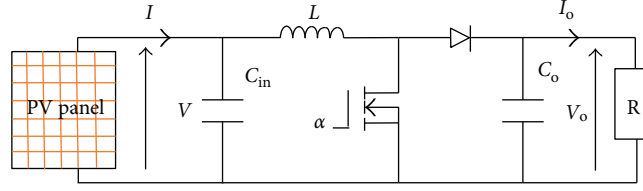


FIGURE 16: Boost converter.

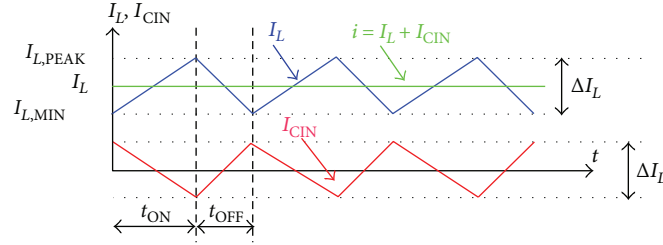


FIGURE 17: Current waveforms of the input capacitor and inductor in CCM.

cycle ( $\alpha$ ) generated by the MPPT controller is put between the panel and the load [23]. The interest of this addition is to remove the mismatch between the panel and the load, and then the PV panel can operate at MPP.

**3.1. Boost Converter Design.** Figure 16 presents the circuit of the boost converter; this converter is used as an adapter between the source and the load [24].

The operation principle of this converter is described by the following equations [25]:

$$\begin{aligned} V_O &= \frac{V}{(1-\alpha)}, \\ I_O &= I(1-\alpha). \end{aligned} \quad (5)$$

By using (5), (6) is obtained, which is the relationship between the resistance seen by the PV panel ( $R_{eq}$ ) and the load resistance ( $R$ ). Hence, based on this equation, the MPPT controller can find the optimum  $\alpha$  to remove the mismatch between the load and MPP. Therefore, The boost converter is required to get maximum power available from the panel.

$$R_{eq} = \frac{V}{I} = \frac{V_O(1-\alpha)^2}{I_O} = R(1-\alpha)^2. \quad (6)$$

**3.1.1. Selection of the Inductor.** The choice of the inductor can directly influence the performance of the boost converter. Moreover, the selection of the inductance is a trade-off between its cost, its size, and the inductor current ripple. A higher inductance value results in a minor inductance current ripple; however, that results in a higher cost and larger inductor's size, which means a larger PCB surface.

By the way, the inductance value can be given as follows: During  $T_{ON}$  state,

$$V = L \frac{\Delta I_L}{T_{ON}} \Rightarrow L = \frac{V\alpha}{\Delta I_L F}, \quad (7)$$

where  $\Delta I_L$  can be computed as below, and  $r$  is the inductor current ripple ratio, which is optimal in the range [0.3, 0.5] [26]:

$$\Delta I_L = r \times I. \quad (8)$$

Therefore, the optimum inductor value can be computed by using

$$L \geq \frac{V\alpha}{rIF}. \quad (9)$$

Based on Figure 17, in order to guarantee the performance of boost converter in the continuous conduction mode, the following equation must be verified:

$$I \geq \frac{\Delta I_L}{2} \Rightarrow \Delta I_L \leq 2I. \quad (10)$$

Therefore,

$$L \geq \frac{\alpha(1-\alpha)^2 R}{2F}. \quad (11)$$

**3.1.2. Selection of the Output Capacitor.** The choice of the output capacitor is made by using output voltage ripple as follows:

During  $T_{ON}$ ,

$$I_O = C_O \frac{\Delta V_O}{T_{ON}} \Rightarrow C_O = \frac{\alpha I_O}{\Delta V_O F}. \quad (12)$$

Therefore, the output capacitor value can be calculated as below, where the desired  $\Delta V_O$  equals to 2% of output voltage [24]:

$$C_O \geq \frac{\alpha}{0.02 \times F \times R}. \quad (13)$$

**3.1.3. Selection of the Input Capacitor.** An input capacitor is used to decrease the input voltage ripple and to deliver an alternative current to the inductor. The input voltage ripple

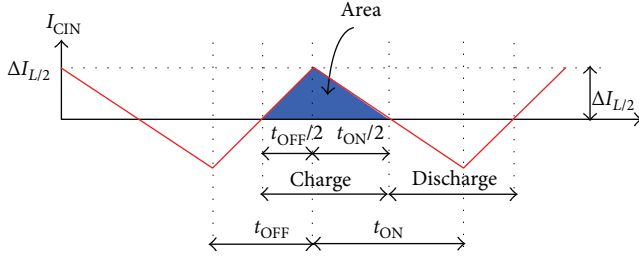


FIGURE 18: Current waveforms of the input capacitor in CCM.

matches to the charge voltage during the charge phase of the capacitor, and during this phase,  $I_{Cin}$  is greater than zero, so this phase is illustrated by the blue area in Figure 18; therefore, this area is used to calculate the input capacitor as follows:

$$I_{Cin} = C_{in} \frac{\Delta V}{\Delta t} \Rightarrow \Delta V = \frac{I_{Cin} \Delta t}{C_{in}}. \quad (14)$$

Based on Figure 18, and by using (14):

$$\Delta V = \frac{\Delta I_L}{8FC_{in}} \Rightarrow C_{in} = \frac{\Delta I_L}{8F\Delta V} = \frac{V\alpha}{8F^2L\Delta V}. \quad (15)$$

Therefore, the input capacitor can be calculated by (16), where the desired  $\Delta V$  equals to 1% of input voltage [27]:

$$C_{in} \geq \frac{\alpha}{8 \times F^2 \times L \times 0.01}. \quad (16)$$

The design of the used boost is presented in Table 2.

**3.2. Problem with the Conventional INC Algorithm.** A good MPPT algorithm balances between the tracking speed and steady-state performance. In accordance with these requirements, the INC algorithm can be used even if it can fail in some cases [20] and in this study, it will be modified in order to improve its performance. INC algorithm is founded in the fact that slope of  $P$ - $V$  characteristic is zero at the MPP [28]. Therefore, this algorithm can be modeled as follows:

$$\begin{aligned} \frac{dP}{dV} &= 0 \quad \text{at MPP,} \\ \frac{dP}{dV} &> 0 \quad \text{left to MPP,} \\ \frac{dP}{dV} &< 0 \quad \text{right to MPP.} \end{aligned} \quad (17)$$

Since

$$\frac{dP}{dV} = \frac{d(IV)}{dV} = V \frac{dI}{dV} + I; \quad (18)$$

then,

$$\frac{dI}{dV} = -\frac{I}{V} \quad \text{at MPP,} \quad (19)$$

$$\frac{dI}{dV} > -\frac{I}{V} \quad \text{left to MPP,} \quad (20)$$

TABLE 2: Design of the boost converter.

Parameters	Values
$L$	1.2 mH
$C_{in}$	75 $\mu$ F
$C_O$	75 $\mu$ F
$F$	10 kHz
$R$	50 $\Omega$
$\alpha_{MPP}$	0.69

$$\frac{dI}{dV} < -\frac{I}{V} \quad \text{right to MPP.} \quad (21)$$

The flowchart of the INC algorithm is presented in Figure 19 [28]. This algorithm measures the current and voltage of the panel. If (21) is met, the duty cycle is increased, and vice versa if (20) is met. Then, there is nothing to do if (19) is met. Therefore, theoretically, if MPP is reached, there is no more perturbation of  $\alpha$ ; consequently, steady-state oscillations are decreased, and that is the main advantage of INC algorithm.

However, the conventional INC algorithm fails to make a good decision when the irradiance is suddenly increased [20]. As presented in Figure 20, once the solar irradiance is at 500 W/m<sup>2</sup> and the PV system operates at load<sub>2</sub>, the INC technique controls the PV system in order to reach the MPP (point B). When the irradiance is increased to 1000 W/m<sup>2</sup>, load<sub>2</sub> will lead the system to point G in  $I$ - $V$  characteristic, which matches to point C in  $P$ - $V$  characteristic. The INC technique calculates the slope between point C and point B which is positive. Therefore, the INC algorithm will decrease the duty cycle and consequently, the PV panel voltage will be increased. But since the MPP of 1000 W/m<sup>2</sup> is at point A, and the slope between point A and C is negative, then the PV panel voltage should have been decreased in order to reach point A, instead of increase voltage and recede from point A as made by the conventional INC algorithm. In addition, as presented in Figure 6, generally when the solar irradiance increases, the MPP moves to the right and consequently, the same problem will occur.

Conversely, this weakness does not happen if the solar irradiation is decreased. Because as shown in Figure 20, the slope is positive between point A and D, and also between point B and D.

**3.3. Modified INC Algorithm.** Based on the above analysis, it is noted that when the solar irradiance increases, both the voltage and the current are increased. Therefore, the sudden increase in solar irradiation can be detected, by checking if the MPP was reached and both the voltage and current are increased. Therefore, a permitted error is accepted (22) to detect that the MPP is reached.

$$\left| \frac{dI}{dV} + \frac{I}{V} \right| < 0.07. \quad (22)$$

The proposed algorithm is presented in Figure 21. So as shown, the addition is the check if the MPP was reached by using (22), then set Var to one. After that, when (22) is

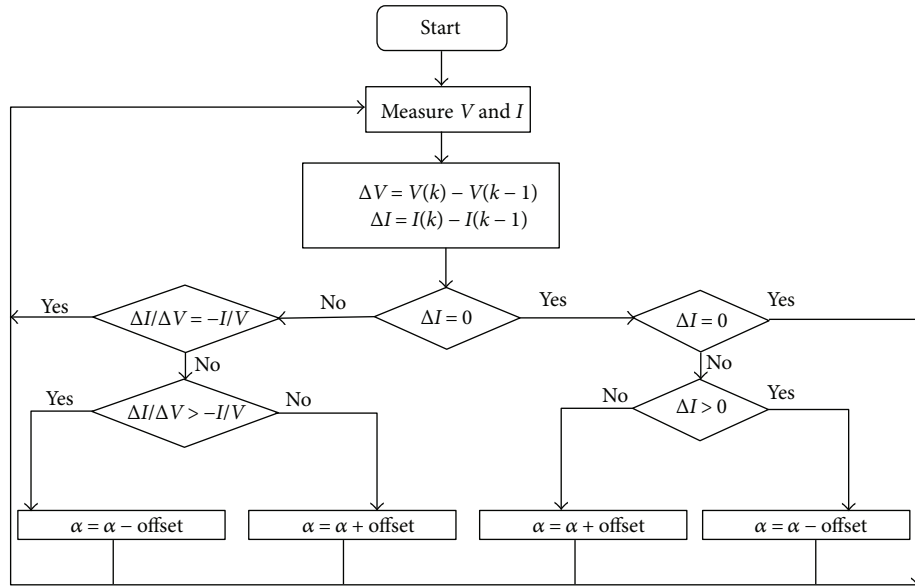


FIGURE 19: Flowchart of INC algorithm.

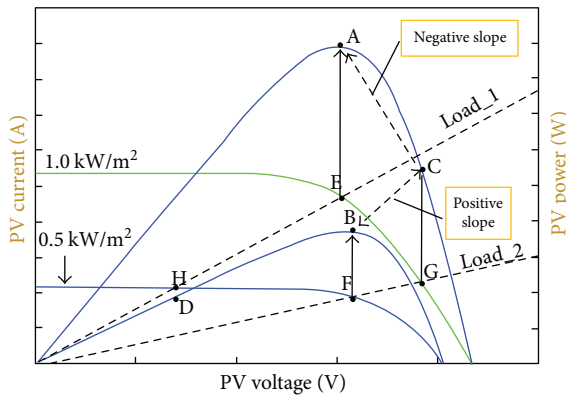


FIGURE 20: P-V and I-V curves for solar irradiation 500 W/m<sup>2</sup> and 1000 W/m<sup>2</sup>.

not met and Var is one, the proposed technique checks if both voltage and current are increased; in this case, the duty cycle is increased instead of decreased as made by the conventional algorithm. Hence, the INC algorithm is modified to overcome the incorrect decision made by the conventional algorithm when the irradiance is increased.

#### 4. Results and Discussions

The test was made for the conventional and the proposed techniques. At first, the solar irradiance is suddenly increased from 500 W/m<sup>2</sup> to 1000 W/m<sup>2</sup> at  $t=0.11$  s, and then it is decreased from 1000 W/m<sup>2</sup> to 500 W/m<sup>2</sup> at  $t=0.23$  s. Figure 22 shows the test result of the conventional technique, and Figure 23 shows the test result of the proposed technique. Therefore, as shown in these figures, the steady-state oscillations are minimized by using the proposed algorithm and admit an error equals to 0.07. Contrary to

the conventional algorithm, the power oscillates between (28.5–29.8 W), and this can generate a loss in PV energy.

In addition, as presented in Figure 22, by using the conventional algorithm, when solar irradiance is suddenly increased, the power diverges with a value greater than 62 W and after that, the conventional INC reverses the direction and the power diverges with a value lower than 56 W; and like that, the system takes a long time to converge around MPP that is due to the wrong decision made by the conventional technique. Also, even if the MPP is reached, the power oscillates between (59–61 W). On the other side, as presented in Figure 23, the proposed technique detects the fast increase of irradiance and makes a correct decision in duty cycle. As a result, the power converges to the new MPP from the first step and it is maintained at it (60 W). In addition, it only needs 0.001 s to reach the MPP. Hence, by using the proposed INC, the power converges faster compared with the conventional algorithm which needs more time to reach the MPP.

Table 3 summarizes a comparison of the proposed technique to other improved INC techniques proposed in the scientific literature in term of the oscillation level, tracking efficiency, the response time during sudden increase in irradiance, and if the technique makes an incorrect decision under sudden increase of irradiance. As presented, the proposed technique shows a very fast tracking speed, a higher efficiency, and neglected oscillations around the MPP compared to other techniques. Thus, only the proposed algorithm and that proposed in [29] make a correct decision under sudden increase of irradiance, contrary to the conventional technique and those proposed in [30, 31] which make an incorrect decision.

#### 5. Conclusion

In this paper, PV panel’s parameters are found using Math-Works tool (PV array); hence, by using these parameters, a



TABLE 3: Comparison of the proposed algorithm with other improved incremental conductance algorithms proposed in scientific literature.

Technique	Oscillation level	Efficiency (%)	Response time during sudden increase in irradiation	Incorrect decision under sudden increase of irradiation
Conventional	2.5 W	96	Slow	Yes
[29]	1 W	96.40	Fast	No
[30]	1.5 W	98.5	Fast	Yes
[31]	1 W	97.5	Medium	Yes
Proposed	Neglected	98.8	Very fast	No

PV panel and a PV array are modeled, and the results show that the model is in accordance with experimental data of the used panel (MSX-60). In addition, a modified INC algorithm which can overcome the confusion faced by the conventional INC technique is proposed in this paper. As a result, the tests show that the modified technique detects the fast increase of irradiation and makes a correct decision, contrary to the conventional technique. Moreover, by using the modified algorithm, steady-state oscillations are almost neglected. Hence, the loss of energy is minimized; consequently, the efficiency is equal to 98.8% instead of 96% obtained by the conventional technique.

As a perspective, the modified INC algorithm can be more improved and then implemented in an embedded hardware device.

## Nomenclature

$a$ :	Diode's ideality factor
$I$ :	Output current of the panel (A)
$I_s$ :	Diode saturation current (A)
$I_{ph}$ :	Panel photocurrent (A)
$G$ :	Solar irradiation ( $W/m^2$ )
$K$ :	Boltzmann constant ( $J \cdot K^{-1}$ )
$q$ :	Electron charge (C)
$R$ :	The load ( $\Omega$ )
$R_{eq}$ :	The resistance seen by the panel ( $\Omega$ )
$R_s$ :	Series resistance ( $\Omega$ )
$R_{sh}$ :	Shunt resistance ( $\Omega$ )
$T$ :	Junction temperature (K)
$V$ :	Output voltage of the panel (V)
$V_O$ :	Output voltage of the boost converter (V)
$I_O$ :	Output current of the boost converter (A)
$F$ :	Switching frequency (Hz)
$\Delta V$ :	Input voltage ripple of the boost converter (V)
$\Delta V_O$ :	Output voltage ripple of the boost converter (V)
$\Delta I_L$ :	Inductor current ripple (A).

## Greek Letters

$\alpha$ : Duty cycle.

## Abbreviations

CCM:	Continuous conduction mode
FSCC:	Fractional short-circuit current
FOCV:	Fractional open-circuit voltage
INC:	Incremental conductance
MPP:	Maximum power point

MPPT: Maximum power point tracking

P&O: Perturb and observe

PV: Photovoltaic

STC: Standard test conditions.

## Conflicts of Interest

The authors declare that they have no conflicts of interest.

## References

- [1] H. Patel and V. Agarwal, "MATLAB-based modeling to study the effects of partial shading on PV array characteristics," *IEEE Transactions on Energy Conversion*, vol. 23, no. 1, pp. 302–310, 2008.
- [2] S. Motahhir, A. Chalh, A. Ghzizal, S. Sebti, and A. Derouich, "Modeling of photovoltaic panel by using proteus," *Journal of Engineering Science and Technology Review*, vol. 10, no. 2, pp. 8–13, 2017.
- [3] S. Motahhir, A. El Ghzizal, S. Sebti, and A. Derouich, "Proposal and implementation of a novel perturb and observe algorithm using embedded software," in *2015 3rd International Renewable and Sustainable Energy Conference (IRSEC)*, pp. 1–5, Marrakech, Morocco, December 2015.
- [4] H. S. Rauschenbach, *Solar Cell Array Design Handbook*, Van Nostrand Reinhold, 1980.
- [5] N. Barth, R. Jovanovic, S. Ahzi, and M. A. Khaleel, "PV panel single and double diode models: optimization of the parameters and temperature dependence," *Solar Energy Materials and Solar Cells*, vol. 148, pp. 87–98, 2016.
- [6] K. Nishioka, N. Sakitani, Y. Uraoka, and T. Fuyuki, "Analysis of multicrystalline silicon solar cells by modified 3-diode equivalent circuit model taking leakage current through periphery into consideration," *Solar Energy Materials and Solar Cells*, vol. 91, no. 13, pp. 1222–1227, 2007.
- [7] N. Yildiran and E. Tacer, "Identification of photovoltaic cell single diode discrete model parameters based on datasheet values," *Solar Energy*, vol. 127, pp. 175–183, 2016.
- [8] K. Ishaque, Z. Salam, S. Mekhilef, and A. Shamsudin, "Parameter extraction of solar photovoltaic modules using penalty-based differential evolution," *Applied Energy*, vol. 99, pp. 297–308, 2012.
- [9] K. Ishaque and Z. Salam, "An improved modeling method to determine the model parameters of photovoltaic (PV) modules using differential evolution (DE)," *Solar Energy*, vol. 85, no. 9, pp. 2349–2359, 2011.
- [10] M. F. AlHajri, K. M. El-Naggar, M. R. AlRashidi, and A. K. Al-Othman, "Optimal extraction of solar cell parameters using pattern search," *Renewable Energy*, vol. 44, pp. 238–245, 2012.

- [11] Mathworks, *PV Array*, 2015, Mai 2017, <https://fr.mathworks.com/help/physmod/sps/powersys/ref/pvarray.html>.
- [12] C. Carrero, J. Amador, and S. Arnaltes, "A single procedure for helping PV designers to select silicon PV modules and evaluate the loss resistances," *Renewable Energy*, vol. 32, no. 15, pp. 2579–2589, 2007.
- [13] T. Radjai, L. Rahmani, S. Mekhilef, and J. P. Gaubert, "Implementation of a modified incremental conductance MPPT algorithm with direct control based on a fuzzy duty cycle change estimator using dSPACE," *Solar Energy*, vol. 110, pp. 325–337, 2014.
- [14] J. Ahmed and Z. Salam, "A modified P&O maximum power point tracking method with reduced steady-state oscillation and improved tracking efficiency," *IEEE Transactions on Sustainable Energy*, vol. 7, no. 4, pp. 1506–1515, 2016.
- [15] A. Amir, J. Selvaraj, and N. A. Rahim, "Study of the MPP tracking algorithms: focusing the numerical method techniques," *Renewable and Sustainable Energy Reviews*, vol. 62, pp. 350–371, 2016.
- [16] A. Gupta, Y. K. Chauhan, and R. K. Pachauri, "A comparative investigation of maximum power point tracking methods for solar PV system," *Solar Energy*, vol. 136, pp. 236–253, 2016.
- [17] D. Verma, S. Nema, A. M. Shandilya, and S. K. Dash, "Maximum power point tracking (MPPT) techniques: recapitulation in solar photovoltaic systems," *Renewable and Sustainable Energy Reviews*, vol. 54, pp. 1018–1034, 2016.
- [18] J. P. Ram, T. S. Babu, and N. Rajasekar, "A comprehensive review on solar PV maximum power point tracking techniques," *Renewable and Sustainable Energy Reviews*, vol. 67, pp. 826–847, 2017.
- [19] S. Motahhir, A. El Ghzizal, S. Sebti, and A. Derouich, "Shading effect to energy withdrawn from the photovoltaic panel and implementation of DMPPT using C language," *International Review of Automatic Control*, vol. 9, no. 2, pp. 88–94, 2016.
- [20] K. S. Tey and S. Mekhilef, "Modified incremental conductance MPPT algorithm to mitigate inaccurate responses under fast-changing solar irradiation level," *Solar Energy*, vol. 101, pp. 333–342, 2014.
- [21] Solarex MSX60 and MSX64 photovoltaic panel, data-sheet1998, April 2017, <https://www.solarelectricsupply.com/media/custom/upload/Solarex-MSX64.pdf>.
- [22] F. Bayrak, G. Ertürk, and H. F. Oztop, "Effects of partial shading on energy and exergy efficiencies for photovoltaic panels," *Journal of Cleaner Production*, vol. 164, pp. 58–69, 2017.
- [23] S. Motahhir, A. El Ghzizal, S. Sebti, and A. Derouich, "MIL and SIL and PIL tests for MPPT algorithm," *Cogent Engineering*, vol. 4, p. 1378475, 2017.
- [24] S. Sivakumar, M. J. Sathik, P. S. Manoj, and G. Sundararajan, "An assessment on performance of DC–DC converters for renewable energy applications," *Renewable and Sustainable Energy Reviews*, vol. 58, pp. 1475–1485, 2016.
- [25] N. Mohan and T. M. Undeland, *Power Electronics: Converters, Applications, and Design*, John Wiley & Sons, 2007.
- [26] S. Maniktala, *Switching Power Supplies A-Z*, Elsevier, 2012.
- [27] M. H. Rashid, *Power Electronics: Circuits, Devices, and Applications*, Pearson Education India, 2009.
- [28] A. Loukriz, M. Haddadi, and S. Messalti, "Simulation and experimental design of a new advanced variable step size incremental conductance MPPT algorithm for PV systems," *ISA Transactions*, vol. 62, pp. 30–38, 2016.
- [29] A. Belkaid, I. Colak, and O. Isik, "Photovoltaic maximum power point tracking under fast varying of solar radiation," *Applied Energy*, vol. 179, pp. 523–530, 2016.
- [30] M. A. G. De Brito, L. Galotto, L. P. Sampaio, G. de Azevedo e Melo, and C. A. Canesin, "Evaluation of the main MPPT techniques for photovoltaic applications," *IEEE Transactions on Industrial Electronics*, vol. 60, no. 3, pp. 1156–1167, 2013.
- [31] P. C. Sekhar and S. Mishra, "Takagi–Sugeno fuzzy-based incremental conductance algorithm for maximum power point tracking of a photovoltaic generating system," *IET Renewable Power Generation*, vol. 8, no. 8, pp. 900–914, 2014.

